Primordial black hole formation from massless scalar isocurvature

Chul-Moon Yoo,[1,*] Tomohiro Harada,[2,†] Shin'ichi Hirano,[1,‡] Hirotada Okawa,[3,§] and Misao Sasaki[4,5,6,‖]

[1]*Division of Particle and Astrophysical Science, Graduate School of Science, Nagoya University,*
Nagoya 464-8602, Japan
[2]*Department of Physics, Rikkyo University, Toshima, Tokyo 171-8501, Japan*
[3]*Waseda Institute for Advanced Study (WIAS), Waseda University, Shinjuku, Tokyo 169-0051, Japan*
[4]*Kavli Institute for the Physics and Mathematics of the Universe (WPI), University of Tokyo,*
Kashiwa 277-8583, Japan
[5]*Center for Gravitational Physics, Yukawa Institute for Theoretical Physics, Kyoto University,*
Kyoto 606-8502, Japan
[6]*Leung Center for Cosmology and Particle Astrophysics, National Taiwan University,*
Taipei 10617, Taiwan

We numerically study the primordial black hole (PBH) formation by an isocurvature perturbation of a massless scalar field on super Hubble scales in the radiation-dominated Universe. As a first step we perform simulations of spherically symmetric configurations. For the initial condition, we employ the spatial gradient expansion and provide the general form of the growing mode solutions valid up through the second order in this expansion. The initial scalar field profile is assumed to be Gaussian with a characteristic comoving wave number k; $\sim \exp(-k^2 R^2)$, where R is the radial coordinate. We find that a PBH is formed for a sufficiently large amplitude of the scalar field profile. Nevertheless, we find that the late time behavior of the gravitational collapse is dominated by the dynamics of the fluid but not by the scalar field, which is analogous to the PBH formation from an adiabatic perturbation in the radiation-dominated Universe.

I. INTRODUCTION

Recent technological advances opened the era of precision cosmology. The resolution which we can access through observations is getting finer and finer, and we now have a fairly accurate picture of the primordial Universe based on the inflationary Universe scenario. However, the accessible range of scales through cosmological observations such as the cosmic microwave background and the large scale structure is very limited, and only little is known about the primordial state of the Universe on small scales, say, on comoving scales smaller than the Galactic scale

In this situation, recently primordial black holes (PBHs) have been attracting a lot of attention. The possible existence of PBHs was suggested about half a century ago [1,2]. There has been a renewed interest in PBHs thanks in particular to the progress in gravitational wave astrophysics and cosmology (e.g., see Refs. [3,4] for reviews on PBHs). Theoretically, many models which

produce a substantial amount of PBHs have been proposed in the context of the inflationary Universe, or in alternative scenarios.

In most of these models, the PBH formation is attributed to the curvature perturbation generated during inflation. In other words, only the single adiabatic degree of freedom has been considered, while isocurvature degrees of freedom which may play important roles in a Universe consisting of multifluids have been largely ignored. Only quite recently, the PBH formation from isocurvature perturbations of the cold dark matter was considered [5] (see also Ref. [6] for the possible detection of gravitational waves from large dark matter isocurvature).

In the case of the conventional PBH formation scenario in the radiation-dominated Universe, numerical simulations of the PBH formation are one of the crucial elements to obtain accurate theoretical predictions (see, e.g., [7–17]). It is also certainly true for the case of PBH formation from isocurvature perturbations. In this paper, we make a first attempt to perform such simulations by considering an isocurvature perturbation of a massless scalar field in the radiation-dominated Universe. We assume spherical symmetry and consider the Gaussian spatial profile, $\phi(R) = \mu \exp(-k^2 R^2/6)$, as the initial scalar field configuration, where μ is the amplitude, k is the characteristic

[*]yoo@gravity.phys.nagoya-u.ac.jp
[†]harada@rikkyo.ac.jp
[‡]hirano.shinichi@a.mbox.nagoya-u.ac.jp
[§]h.okawa@aoni.waseda.jp
[‖]misao.sasaki@ipmu.jp

wave number of the perturbation, and R is the radial coordinate.

To begin with, it is not totally apparent if a PBH can be formed from an isocurvature perturbation of a massless scalar field. To formulate the problem in a consistent way, we have to set the appropriate initial condition for a primordially isocurvature perturbation. For this purpose, we employ the spatial gradient expansion, which is valid for perturbations on scales much larger than the Hubble horizon scale. Thus, we first perform the long-wavelength expansion of the field equations by taking the existence of the massless scalar field into account. Due to the isocurvature nature of perturbations, the zeroth order solution for the metric should be given by the standard homogeneous and isotropic radiation-dominated Universe. Thus, we can easily identify the leading order isocurvature perturbation and obtain the general solution for the isocurvature growing mode up through the next leading order terms in gradient expansion, which arise from the spatial gradients of the scalar field. These next leading order terms are the ones that gradually induce nontrivial perturbations in the geometry, and may eventually lead to PBH formation. In fact, we explicitly show that this isocurvature growing mode can result in the formation of a PBH if the initial amplitude μ is sufficiently large.

This paper is organized as follows. We write down all relevant equations in the form of the cosmological $3 + 1$ decomposition in Sec. II A following Refs. [7,18]. Then, performing the gradient expansion, we derive the growing mode solution for a massless scalar field isocurvature perturbation in Sec. II B. The spherically symmetric numerical simulations are described in Sec. III. The numerical code, the initial data, the time evolution of dynamical quantities, the evolution of the PBH mass after the formation, and the scaling of the black hole mass near the threshold are discussed in Secs. III A–III E, respectively. Section IV is devoted to a summary and discussion.

Throughout this paper, we use the geometrized units in which both the speed of light and Newton's gravitational constant are set to unity, $c = G = 1$.

II. LONG-WAVELENGTH APPROXIMATION FOR A PERFECT FLUID-MASSLESS SCALAR SYSTEM

A. Equations of motion

Let us write down the cosmological $3 + 1$ form of the equations of motion given in Ref. [18] adding a massless scalar field. Since there is no direct coupling between the scalar field and the fluid, the equations of motion can be obtained by simply adding the contribution of the massless scalar field into the stress-energy tensor and additionally considering the dynamical equations for the massless scalar field. In the following, we recapitulate the Einstein equations and the conservation and Euler equations from Ref. [18] (see also Ref. [7]). We use the notation in which the Greek indices run over 0 to 3, and the Latin indices over 1 to 3. The reference spatial metric associated with the coordinates x^i will be expressed as η_{ij}, where x^i are not necessarily Cartesian. The Cartesian coordinates are denoted by $X^i = (X, Y, Z)$.

The Hamiltonian and momentum constraints are given as follows:

$$\tilde{\triangle}\psi = \frac{\tilde{\mathcal{R}}_k^k}{8}\psi - 2\pi\psi^5 a^2 E - \frac{\psi^5 a^2}{8}\left(\tilde{A}_{ij}\tilde{A}^{ij} - \frac{2}{3}K^2\right), \quad (1)$$

$$\tilde{\mathcal{D}}^j(\psi^6\tilde{A}_{ij}) - \frac{2}{3}\psi^6\tilde{\mathcal{D}}_i K = 8\pi J_i\psi^6, \quad (2)$$

where $\tilde{\triangle}$ is the Laplacian with respect to the conformal metric $\tilde{\gamma}_{ij}$ which is related to the spatial metric γ_{ij} as $\gamma_{ij} = \psi^4 a^2 \tilde{\gamma}_{ij}$ with $\det(\tilde{\gamma}) = \eta := \det(\eta)$ and a being the scale factor in the reference Universe. $\tilde{\mathcal{R}}_{ij}$ is the Ricci tensor with respect to the conformal metric $\tilde{\gamma}_{ij}$. E and J_i are the energy density and momentum density for the Eulerian observer defined by $E := n_\mu n_\nu T^{\mu\nu}$ and $J_i := -\gamma_{i\mu} n_\nu T^{\mu\nu}$ with n_μ and $T^{\mu\nu}$ being the unit vector normal to the time slice and total stress-energy tensor, respectively. $\tilde{A}_{ij}$ is related to the traceless part A_{ij} of the extrinsic curvature K_{ij} as $A_{ij} = \psi^4 a^2 \tilde{A}_{ij}$. We raise the Latin lowercase indices $i, j, k, \ldots$ of tilded quantities by $\tilde{\gamma}^{ij}$, and $\tilde{\mathcal{D}}_i$ is the covariant derivative with respect to $\tilde{\gamma}_{ij}$.

The evolution equations for ψ, $\tilde{\gamma}_{ij}$, $K = \gamma^{ij}K_{ij}$, and $\tilde{A}_{ij}$ are given as

$$(\partial_t - \mathcal{L}_\beta)\psi = -\frac{\dot{a}}{2a}\psi + \frac{\psi}{6}(-\alpha K + \bar{\mathcal{D}}_k\beta^k), \quad (3)$$

$$(\partial_t - \mathcal{L}_\beta)\tilde{\gamma}_{ij} = -2\alpha\tilde{A}_{ij} - \frac{2}{3}\tilde{\gamma}_{ij}\bar{\mathcal{D}}_k\beta^k. \quad (4)$$

$$(\partial_t - \mathcal{L}_\beta)K = \alpha\left(\tilde{A}_{ij}\tilde{A}^{ij} + \frac{1}{3}K^2\right) - D_k D^k\alpha + 4\pi\alpha(E + S_k^k), \quad (5)$$

$$(\partial_t - \mathcal{L}_\beta)\tilde{A}_{ij} = \frac{1}{a^2\psi^4}\left[\alpha\left(\mathcal{R}_{ij} - \frac{\gamma_{ij}}{3}\mathcal{R}\right) - \left(D_i D_j\alpha - \frac{\gamma_{ij}}{3}D_k D^k\alpha\right)\right]$$
$$+ \alpha(K\tilde{A}_{ij} - 2\tilde{A}_{ik}\tilde{A}_j^k) - \frac{2}{3}(\bar{\mathcal{D}}_k\beta^k)\tilde{A}_{ij} - \frac{8\pi\alpha}{a^2\psi^4}\left(S_{ij} - \frac{\gamma_{ij}}{3}S_k^k\right), \quad (6)$$

where α is the lapse function, $\mathcal{L}_\beta$ is the Lie derivative associated with the shift vector β^i, and D_i is the covariant derivative with respect to γ_{ij}.

The conservation of the stress-energy tensor for a perfect fluid can be rewritten as follows:

$$[\psi^6 a^3\{(\rho+p)\Gamma^2 - p\}]_{,t} + \frac{1}{\sqrt{\eta}}[\sqrt{\eta}\psi^6 a^3\{(\rho+p)\Gamma^2 - p\}v^l]_{,l}$$

$$= -\frac{1}{\sqrt{\eta}}[\sqrt{\eta}\psi^6 a^3 p(v^l + \beta^l)]_{,l} + \alpha\psi^6 a^3 pK - \alpha^{-1}\alpha_{,l}\psi^6 a^3\Gamma^2(\rho+p)(v^l + \beta^l)$$

$$+ \alpha^{-1}\psi^{10}a^5\Gamma^2(\rho+p)(v^l + \beta^l)(v^m + \beta^m)\left(\tilde{A}_{lm} + \frac{\tilde{\gamma}_{lm}}{3}K\right), \tag{7}$$

$$(\Gamma\psi^6 a^3(\rho+p)u_j)_{,t} + \frac{1}{\sqrt{\eta}}(\sqrt{\eta}\Gamma\psi^6 a^3(\rho+p)v^k u_j)_{,k}$$

$$= -\alpha\psi^6 a^3 p_{,j} + \Gamma\psi^6 a^3(\rho+p)\left(-\Gamma\alpha_{,j} + u_k\beta^k_{,j} - \frac{u_k u_l}{2u^t}\gamma^{kl}_{,j}\right), \tag{8}$$

$$(\Gamma\psi^6 a^3 n)_{,t} + \frac{1}{\sqrt{\eta}}(\sqrt{\eta}\Gamma\psi^6 a^3 n v^k)_{,k} = 0, \tag{9}$$

where ρ, p, and u^μ are the energy density, pressure, and the four-velocity, respectively, of the fluid, by which the fluid stress-energy tensor is given as $T^f_{\mu\nu} = (\rho+p)u_\mu u_\nu + pg_{\mu\nu}$, and v^i and Γ are defined by $v^i = u^i/u^t$ and $\Gamma = \alpha u^t$, respectively.[1]

The field equations for a massless scalar field ϕ are written as

$$(\partial_t - \beta^i\partial_i)\phi = -\alpha\varpi, \tag{10}$$

$$(\partial_t - \beta^i\partial_i)\varpi = -\alpha\triangle\phi - \gamma^{\mu\nu}\partial_\mu\alpha\partial_\nu\phi + \alpha K\varpi, \tag{11}$$

where $\triangle$ is the Laplacian with respect to the spatial metric γ_{ij}. As the stress-energy tensor of ϕ is given by $T^{sc}_{\mu\nu} = \nabla_\mu\phi\nabla_\nu\phi - \frac{1}{2}g_{\mu\nu}\nabla^\lambda\phi\nabla_\lambda\phi$, its contribution to E, J_i and the stress-tensor S_{ij} are given by

$$E^{sc} = n^\mu n^\nu T^{sc}_{\mu\nu} = \frac{1}{2}\varpi^2 + \frac{1}{2}\psi^{-4}a^{-2}\tilde{\gamma}^{ij}\partial_i\phi\partial_j\phi, \tag{12}$$

$$J^{sc}_i = -\gamma_i{}^\mu n^\nu T^{sc}_{\mu\nu} = \varpi\partial_i\phi, \tag{13}$$

$$S^{sc}_{ij} == \gamma_i{}^\mu\gamma_j{}^\nu T^{sc}_{\mu\nu} = \partial_i\phi\partial_j\phi - \frac{1}{2}\tilde{\gamma}_{ij}\tilde{\gamma}^{kl}\partial_k\phi\partial_l\phi$$
$$+ \frac{1}{2}\psi^4 a^2\tilde{\gamma}_{ij}\varpi^2. \tag{14}$$

[1]Γ is denoted by w in Ref. [18].

B. Gradient expansion

We apply the spatial gradient expansion to the equations of motion by introducing the fictitious expansion parameter ϵ associated with the spatial derivative. To be precise, we put the parameter ϵ in front of the spatial partial derivative, e.g., $\partial_i \to \epsilon\partial_i$. For a typical wave number k associated with an inhomogeneity, $\epsilon \sim k/(aH_b)$, where H_b is the background Hubble parameter. In this paper, we assume that the massless scalar field does not contribute to the background metric of the gradient expansion. That is, the only matter component in the background Friedmann-Lemaître-Robertson-Walker (FLRW) Universe is the fluid, which we leave unspecified, though we take it to be the radiation in the numerical simulation. Since the massless scalar can contribute to the stress-energy tensor only through the derivative terms, we may assume the massless scalar field to have the form

$$\phi = \Upsilon(x) + \lambda(t, x), \tag{15}$$

where Υ is assumed to be $\mathcal{O}(1)$ and $\lambda(t, x) = \mathcal{O}(\epsilon)$. This is the most general form of ϕ which makes no leading order contribution to the stress energy tensor, Eq. (12). Then, expanding the scalar field equations, we obtain

$$\partial_t\lambda = -\varpi + \mathcal{O}(\epsilon^2), \tag{16}$$

$$\partial_t\varpi = K_b\varpi + \mathcal{O}(\epsilon^2). \tag{17}$$

Using the fact that $K_b = -3\dot{a}/a$, we obtain the general solution to Eqs. (16) and (17) as follows:

$$\lambda = \lambda_1(x) + \lambda_2(x)\int a^{-3}dt + \mathcal{O}(\epsilon^2). \tag{18}$$

The second term is the decaying mode, and we drop it. Since the first term can be absorbed into the leading term $\Upsilon(x)$, we conclude

$$\lambda(t, \boldsymbol{x}) = \mathcal{O}(\epsilon^2). \tag{19}$$

With the above result for the massless scalar field, we find the order counting for the other variables are unchanged from Ref. [18]. To summarize, the expansion orders of the variables are given as follows:

$$\psi = \Psi(\boldsymbol{x})(1 + \xi(t, \boldsymbol{x})) + \mathcal{O}(\epsilon^3), \tag{20}$$

$$\tilde{\gamma}_{ij} = \eta_{ij} + h_{ij} + \mathcal{O}(\epsilon^3), \tag{21}$$

$$K = K_{\rm b}(1 + \kappa) + \mathcal{O}(\epsilon^3), \tag{22}$$

$$\alpha = 1 + \chi + \mathcal{O}(\epsilon^3), \tag{23}$$

$$\beta^i = \mathcal{O}(\epsilon), \tag{24}$$

$$\rho = \rho_{\rm b}(1 + \delta) + \mathcal{O}(\epsilon^3), \tag{25}$$

$$v^i = \mathcal{O}(\epsilon), \tag{26}$$

$$\phi = \Upsilon(\boldsymbol{x}) + \lambda(t, \boldsymbol{x}) + \mathcal{O}(\epsilon^3), \tag{27}$$

$$\varpi = \mathcal{O}(\epsilon^2), \tag{28}$$

where $K_{\rm b} = -3H_{\rm b}$, $\rho_{\rm b} = 3H_{\rm b}^2/(8\pi)$, and $\Psi = \mathcal{O}(1)$. The perturbation variables ξ, h_{ij}, κ, χ and δ are of $\mathcal{O}(\epsilon^2)$. We also find $v^i + \beta^i = \mathcal{O}(\epsilon^3)$ (see Ref. [18] for details).

Hereafter, we fix the gauge as the uniform-mean-curvature slicing ($\kappa = 0$) and the normal coordinates ($\beta^i = 0$), so that $v^i = \mathcal{O}(\epsilon^3)$. We focus on the perfect fluid with the equation of state $p = w\rho$ with constant w. Since we are interested in primordially isocurvature perturbations, we may set $\Psi = 1$, implying that there is no curvature perturbation initially. Then, we obtain the following set of equations:

$$\dot{\delta} + 6\dot{\xi} + 3H_{\rm b}w\chi = \mathcal{O}(\epsilon^4), \tag{29}$$

$$\frac{1}{1 + w}\dot{\delta} + 6\dot{\xi} = \mathcal{O}(\epsilon^4), \tag{30}$$

$$\partial_t[a^3(1 + w)\rho_{\rm b}u_j] = -a^3\rho_{\rm b}[w\partial_j\delta + (1 + w)\partial_j\chi] + \mathcal{O}(\epsilon^5), \tag{31}$$

$$6\dot{\xi} - 3H_{\rm b}\chi = \mathcal{O}(\epsilon^4), \tag{32}$$

$$\rho_{\rm b}\delta + \frac{1}{2}a^{-2}(\mathcal{D}\Upsilon)^2 = \mathcal{O}(\epsilon^4), \tag{33}$$

$$3(1 + w)\chi + (1 + 3w)\delta = \mathcal{O}(\epsilon^4), \tag{34}$$

$$\partial_t h_{ij} = -2\tilde{A}_{ij} + \mathcal{O}(\epsilon^4), \tag{35}$$

$$\partial_t\tilde{A}_{ij} + \frac{3\dot{a}}{a}\tilde{A}_{ij} = -\frac{8\pi}{a^2}\left(\mathcal{D}_i\Upsilon\mathcal{D}_j\Upsilon - \frac{1}{3}\eta_{ij}(\mathcal{D}\Upsilon)^2\right) + \mathcal{O}(\epsilon^4), \tag{36}$$

$$\bar{\mathcal{D}}_i(\Psi\tilde{A}_j^i) = 8\pi(1 + w)\rho_{\rm b}u_j + 8\pi\varpi\mathcal{D}_j\Upsilon + \mathcal{O}(\epsilon^5), \tag{37}$$

$$\partial_t\lambda = -\varpi + \mathcal{O}(\epsilon^3), \tag{38}$$

$$\partial_t\varpi = -a^{-2}\bar{\triangle}\Upsilon - 3H_{\rm b}\varpi, \tag{39}$$

where $(\mathcal{D}\Upsilon)^2 = \eta^{ij}\mathcal{D}_i\Upsilon\mathcal{D}_j\Upsilon$ and $\bar{\triangle} = \eta^{ij}\mathcal{D}_i\mathcal{D}_j$.

Let us solve the above set of equations. The initial condition is given by the scalar field configuration $\phi = \Upsilon(\boldsymbol{x})$. From Eqs. (33) and (34), we find

$$\delta = -\frac{4\pi}{3}\left(\frac{1}{aH_{\rm b}}\right)^2(\mathcal{D}\Upsilon)^2, \tag{40}$$

$$\chi = -\frac{1 + 3w}{3(1 + w)}\delta. \tag{41}$$

From Eq. (32), we obtain

$$\dot{\xi} = \frac{2\pi}{9}\frac{1 + 3w}{1 + w}\frac{1}{a}\left(\frac{1}{aH_{\rm b}}\right)(\mathcal{D}\Upsilon)^2. \tag{42}$$

Integrating this equation and ignoring the constant mode, which corresponds to a nonvanishing curvature perturbation, we obtain

$$\xi = \frac{2\pi}{9}\frac{1}{1 + w}\left(\frac{1}{aH_{\rm b}}\right)^2(\mathcal{D}\Upsilon)^2, \tag{43}$$

where we have used the relation:

$$\frac{\mathrm{d}}{\mathrm{d}t}\left(\frac{1}{aH_{\rm b}}\right)^2 = \frac{1 + 3w}{a^2H_{\rm b}}.$$

One can directly check that the above expressions solve Eqs. (29) and (30). Thus, although we have assumed $\Psi = 1$, ξ at $\mathcal{O}(\epsilon^2)$ does not vanish in general, and may lead to a significant metric perturbation around the horizon entry.

Integrating Eqs. (31), (35), (37), and (39), and dropping the decaying modes, we obtain

$$u_i = -\frac{8\pi}{9}\frac{a}{(1 + w)(5 + 3w)}\left(\frac{1}{aH_{\rm b}}\right)^3\mathcal{D}_i(\mathcal{D}\Upsilon)^2, \tag{44}$$

$$\tilde{A}_{ij} = -\frac{16\pi}{5+3w}\frac{1}{a}\frac{1}{aH_b}\left[\mathcal{D}_i\Upsilon\mathcal{D}_j\Upsilon - \frac{1}{3}\eta_{ij}(\mathcal{D}\Upsilon)^2\right], \quad (45)$$

$$h_{ij} = \frac{32\pi}{(5+3w)(1+3w)}\left(\frac{1}{aH_b}\right)^2\left[\mathcal{D}_i\Upsilon\mathcal{D}_j\Upsilon - \frac{1}{3}\eta_{ij}(\mathcal{D}\Upsilon)^2\right], \quad (46)$$

$$\varpi = -\frac{2}{5+3w}\frac{1}{a}\frac{1}{aH_b}\bar{\triangle}\Upsilon. \quad (47)$$

By using Eqs. (44), (45), and (47), one can show that the momentum constraint Eq. (37) is satisfied. Finally, from Eq. (38), λ is given by

$$\lambda = \frac{2}{(5+3w)(1+3w)}\left(\frac{1}{aH_b}\right)^2\bar{\triangle}\Upsilon. \quad (48)$$

As is explicitly shown in this subsection, once the functional form of $\Upsilon(x)$ is specified, we can solve the equations of motion at each order in the gradient expansion. To summarize, the solution with $\Psi(x) = 1$ but nontrivial $\Upsilon(x)$ is the isocurvature mode, which is of our interest, while the one with $\Upsilon(x) = \text{const}$ but nontrivial $\Psi(x)$ corresponds to the standard curvature perturbation. To be more precise, general growing mode solutions are generated by the set of the functions $\Psi(x)$ and $\Upsilon(x)$ whose spatial variations are initially in the super-horizon regime. As $\Upsilon(x)$ does not contribute to the spacetime curvature up until $O(\epsilon^4)$, while $\Psi(x)$ contributes at $O(\epsilon^2)$, we focus on the perturbations independent of those generated from $\Psi(x)$, which is the definition of the isocurvature mode in this paper.

Before ending this subsection, it is worth defining and evaluating the compaction function of our isocurvature initial condition. Although the distinction of the curvature perturbation component from the isocurvature one at the horizon entry is difficult due to the nonlinear mixing, it is still possible to consider the compaction function for the isocurvature perturbation on superhorizon scales when the curvature component is negligible. Let us define the compaction function for the isocurvature perturbation by $\mathcal{C}(R) \equiv 2\delta M(R)/R$ where $\delta M(R)$ is the energy carried by the scalar field within the radius R. That is, since we have $E^{SC} = \frac{1}{2}a^{-2}(\partial_r\Upsilon)^2 + \mathcal{O}(\epsilon^4)$, we define the compaction function by

$$\mathcal{C}(R) = \frac{4\pi}{R}\int_0^R(\partial_r\Upsilon)^2 r^2 dr. \quad (49)$$

For our initial condition,

$$\mathcal{C}(R) = \frac{4\pi\mu^2}{9R}k^4\int_0^R\exp\left[-\frac{k^2r^2}{3}\right]r^4 dr. \quad (50)$$

The maximum of $\mathcal{C}(R)$ is at $kR \sim 3.5$ with the value $\mathcal{C} \sim 3.5\mu^2$. Thus, if we apply a similar criterion used for

an adiabatic perturbation and assume $\mathcal{C}_{\text{critical}} \sim 1$ for PBH formation, the corresponding critical value of μ would be $\mu \sim 0.53$. As we shall see in the next subsection, this value is fairly close to the actual critical value. This indicates that the compaction function criterion is also useful for initially isocurvature perturbations.

III. NUMERICAL SIMULATION

A. Numerical code

Numerical simulations are performed by using newly developed numerical code based on the $3+1$ dimensional simulation code used in Refs. [17,19]. The $3+1$ dimensional numerical code is modified by implementing the CARTOON method [20], so that the new code is specialized for spherically symmetric systems. That is, we solve the evolution equations only on the Z axis and create the necessary data around it for the time evolution based on the spherical symmetry. We also set the background radiation-dominated, $w = 1/3$. For this purpose, we need to evaluate the physical quantities at off-grid points on the Z axis with interpolation. We implemented the third order spline interpolation to realize the stable time evolution. As in Refs. [17,19], we use the scale-up coordinates with the parameter η, where the ratio of the unit coordinate interval in the Cartesian coordinates near the center is finer by a factor $1+2\eta$ in comparison to that near the boundary (see Ref. [19] for details). The value of η is set $\eta = 40$ except for the simulation shown in Sec. III E, where we set $\eta = 20$ with fixed mesh refinement. When a black hole region is observed, we excise a part of the inner region in the subsequent time evolution.

B. Initial setting

As is shown in Sec. II B, once we specify the functional form of Υ, we obtain the long-wavelength solution for an isocurvature perturbation. In this paper, we consider the following specific spherically symmetric profile of Υ:

$$\Upsilon(R) = \mu\exp\left(-\frac{1}{6}k^2R^2\right)W(R), \quad (51)$$

where $R^2 = X^2 + Y^2 + Z^2$ with X, Y, and Z being the Cartesian coordinates for η_{ij}, and the function $W(R)$ is introduced to make ϕ smoothly vanish at the boundary. The specific form of $W(R)$ is given by [19]

$$W(R) = \begin{cases} 1 & \text{for } 0 \leq R \leq R_W \\ 1 - \frac{((R_W-L)^6-(L-R)^6)^6}{(R_W-L)^{36}} & \text{for } R_W \leq R \leq L, \\ 0 & \text{for } L \leq R \end{cases} \quad (52)$$

where L is the Cartesian radius at the numerical outer boundary and R_W is set to $4L/5$. The amplitude of the inhomogeneity is characterized by the parameter μ, and $1/k$

gives the scale of the inhomogeneity because $\triangle \Upsilon|_{r=0} = -k^2 \Upsilon$. It may be noted, however, if we simply identify the Gaussian profile with the Gaussian window function adopted in the PBH formation from the curvature perturbation, the corresponding comoving wave number would be $k_*^2 = k^2/3$ because the standard Gaussian window function associated with the wave number k_* is defined as $\exp(-k^2/(2k_*^2))$.

We adopt the asymptotically FLRW boundary condition used in Ref. [7], but the constraints are significantly violated on the boundary through the time evolution.[2] Therefore, we terminate the time evolution before the boundary effects influence the formation and evolution of a PBH. At the initial time, the Cartesian radius L at the numerical outer boundary is set to 1 which corresponds to the normalization of the scale factor. We fix the ratio between the wave number k and the initial Hubble parameter H_i as $H_i/k = 5$. The initial value of the background Hubble parameter is set to $50/L$ or $100/L$ depending on the resolution requirement. Namely, we adopt $50/L$ for simulating the PBH formation process, while we adopt $100/L$ for evolving the dynamics after the PBH formation. A smaller value of H_i gives a finer resolution at the center, but the effects of the boundary reach the central region earlier. We define the horizon entry time by t_H by $aH_b|_{t=t_H} = k$, and the horizon mass by $M_H = 1/(2H_b(t_H)) = t_H$.[3]

C. Time evolution of two typical cases

First, let us show two typical cases $\mu = 0.62$ and $\mu = 0.64$ in Figs. 1, 2, and 4. Snapshots of the scalar field, the ratio of the fluid density to the background value, and the lapse function are shown in Fig. 1. It should be noted that the horizontal axis is the scale-up coordinate z, and the initial profile of the scalar field is not Gaussian in this coordinate although it is Gaussian in the coordinate R as is given in Eq. (51). The scalar field initially contributes to the energy density mainly through its spatial gradients, and the energy excess due to the gradient energy is compensated by the under density of the fluid because of the isocurvature condition, $\Psi = 1$ [see Eq. (33)]. The scalar field decays after the horizon entry in both cases.

In Fig. 2, the compactness C (Misner-Sharp mass M_{MS} divided by the half of the area radius) is plotted as a function of z at several moments of time. For the $\mu = 0.64$ case, the fluid energy density forms a sharp peak at the center (see right-middle panel in Fig. 1) and a black hole

apparent horizon ($C = 1$ and $\partial_r C < 0$ in Fig. 2) appears as is explicitly shown in Fig. 2. After the black hole formation, we excise a central region inside the horizon. For the $\mu = 0.62$ case, no black hole formation is observed, and we find that the density wave of the fluid propagates outward. The lapse function for the $\mu = 0.62$ case bounces back to the value close to 1. In Fig. 2, we also find that the cosmological horizon ($C = 1$ and $\partial_r C > 0$ in Fig. 2) always exists and expands outward.

Let us closely look at the time evolution of the energy density around the horizon entry. In Fig. 3, we show the time evolution of the ratio of the scalar field energy density E^{sc} to the fluid energy density E^f (left panel) and the ratio of the total energy density given by $(dM_{MS}/dR_A)/(4\pi R_A^2)$ with R_A being the areal radius to the background energy density ρ_b (right panel), for $\mu = 0.64$. We do not show the $\mu = 0.62$ case because the behaviors are similar to those for $\mu = 0.64$ around the horizon entry. Around the horizon entry, the kinetic energy of the scalar field makes a considerable contribution in the central region, and it gradually decays from $t \sim 10t_H$. Thus, the collapsing dynamics is dominated by the fluid in the late time. The total energy density initially grows together with the energy density of the scalar field and keeps growing after the horizon entry. It is worthy to note that, at the initial time $t = 0.04t_H$, as is shown in Fig. 3, the amplitude of the total energy density perturbation represented by the Misner-Sharp mass is tiny compared to the background energy density. This implies that the peak value of the corresponding compaction function is also tiny. This is the specific character of the isocurvature perturbation, and it can contribute to the nontrivial inhomogeneous geometry only around and after the horizon entry.

In order to show the convergence of the simulation, we also plot the average value of the violation of the Hamiltonian constraint in Fig. 4. We note that the average is taken outside the black hole horizon if it exists. We find that the convergence is roughly quadratic in the spatial resolution. Since we are using a second order scheme in the evaluation of the fluid flux, the order of the convergence is consistent with our procedure.

D. Time evolution of the PBH mass

Let us check the time evolution of the mass of the PBH. Since the energy density of the scalar field is negligible compared to the fluid energy density during and after the collapse, we may expect that the black hole mass obeys the following simple formula firstly proposed by Zel'dovich and Novikov [21] (see also Refs. [22,23] for its extension and numerical fitting):

$$\frac{dM}{dt} = 16\pi FM^2\rho_b, \qquad (53)$$

where ρ_b is the background energy density and F is the constant which determines the accretion efficiency.

---

[2]The constraint violation at the boundary starts to occur when the effects of the inhomogeneity reach the boundary, and the origin of the constraint violation is due to unphysical reflected modes. As far as we know, for the asymptotically FLRW boundary, no established procedure to reduce the unphysical reflected modes has been reported.

[3]As noted in the above, if we use k_* to define the horizon entry in place of k, the corresponding time, and hence the horizon mass, becomes 3 times larger, $t_* = 3t_H$.
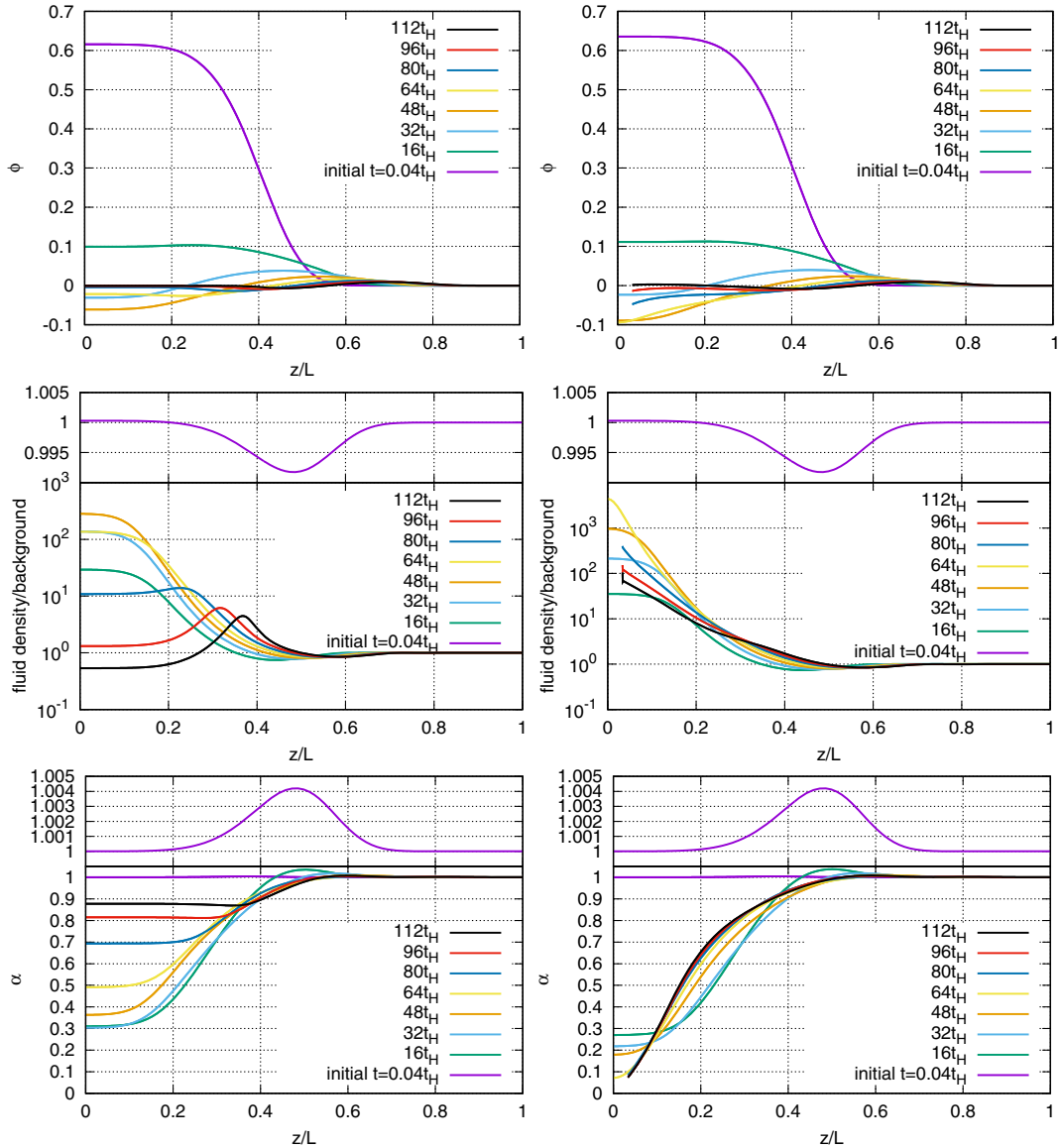
FIG. 1.   Snapshots of the lapse function, scalar field, ratio of the fluid density to the background are shown for $\mu = 0.62$ (left) and $\mu = 0.64$ (right). In the lower two rows, the initial configuration is shown in a different scale.
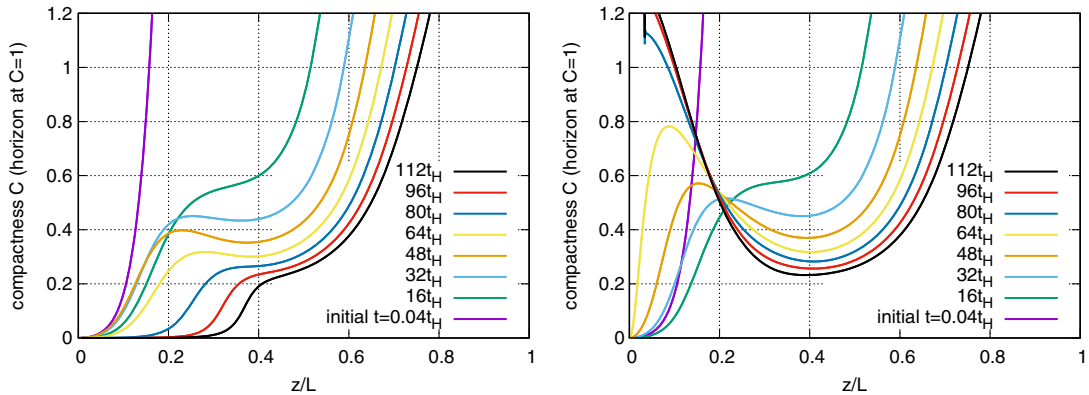

FIG. 2.   Snapshots of the compactness C (Misner-Sharp mass divided by the half of the area radius) are shown for $\mu = 0.62$ (left) and $\mu = 0.64$ (right). For the $\mu = 0.64$ case, the black hole horizon is formed at around $t = 74t_{\rm H}$.
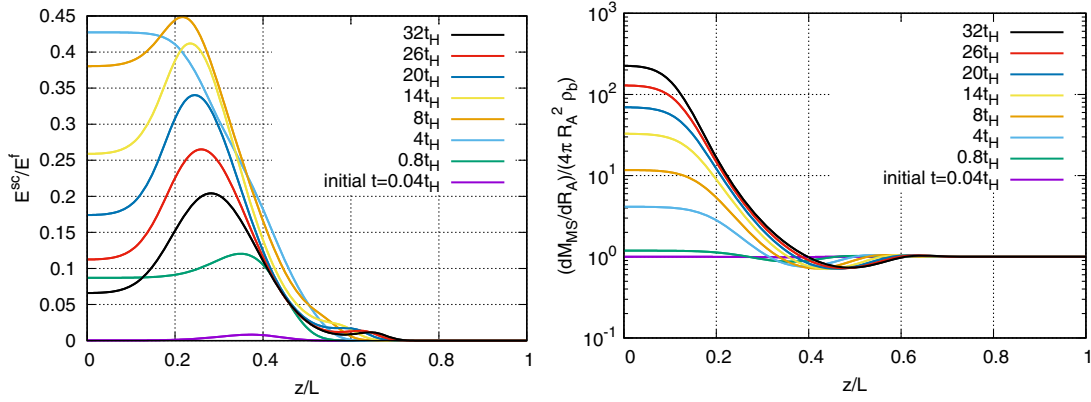
FIG. 3. Snapshots of the ratio of the scalar field energy density to the fluid energy density E^{sc}/E^{f} (left) and the ratio of the total energy density to the background energy density $dM_{MS}/dR_A/(4\pi R_A^2 \rho_b)$, for $\mu = 0.64$.
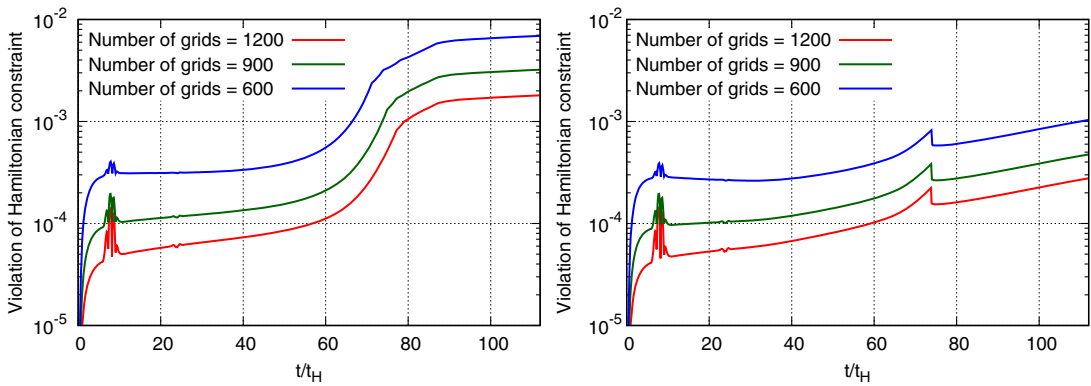

FIG. 4. The average value of the violation of the Hamiltonian constraint with respect to the number of grid points as a function of time, for $\mu = 0.62$ (left) and $\mu = 0.64$ (right). For the $\mu = 0.64$ case, the average is taken outside the black hole horizon after the horizon formation at around $t = 74t_H$.
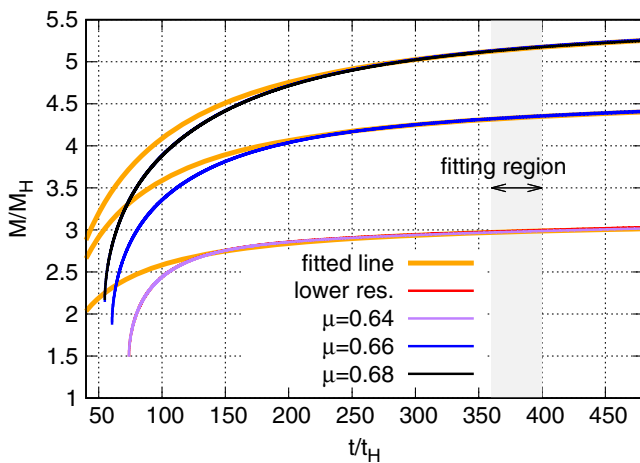

FIG. 5. The time evolution of the black hole mass is shown for each value of μ. The yellow thick lines are fitted lines with the equation (54) which has two parameters M_f and F. The values of these fitting parameters are summarized in Table I. The fitting is performed in the shaded region in the graph.

Integrating this equation for the radiation-dominated Universe, we obtain the following expression:

$$M(t) = \frac{1}{\frac{1}{M_f} + \frac{3F}{2t}}, \quad (54)$$

where M_f is the final mass of the black hole. This formula is expected to be valid in a sufficiently late time after the black hole formation. There are some arguments about the value of F [21,22]. When we compare the formula with a numerical result, the foliation of the time slice should be properly taken into account (see the Appendix for a simple discussion). In this paper, avoiding all these complexities,

TABLE I. The values of F and M_f for each value of μ.

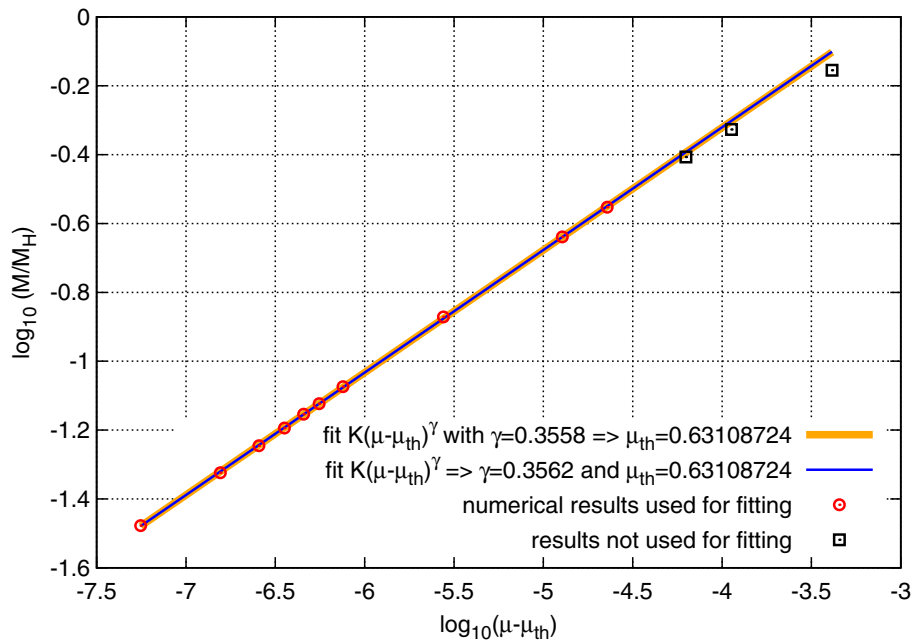| μ	$M_f[M_H]$	F
0.64	3.15	4.65
0.66	4.68	4.32
0.68	5.68	4.56

FIG. 6. The mass of the primordial black hole at the formation time is plotted as a function of the initial amplitude of the massless scalar field. The solid blue line is the fitted line of the functional form $M/M_H = \mathcal{K}(\mu - \mu_{\text{th}})^\gamma$, and the best fit value of γ is given by 0.3562. The thick orange line is the fitted line with γ fixed to be 0.3558. For the fitting, we used the lower ten points indicated by the red circle where the scaling relation seems applicable. We obtain $\mu_{\text{th}} \simeq 0.63108724$ in the fitting for both cases, and $\mathcal{K} \simeq 12.6$ and 12.7 for the orange and blue lines, respectively.

we simply treat the constant F as a fitting parameter together with M_{f}.

We performed numerical simulations for the three cases: $\mu = 0.64$, 0.66, and 0.68. The time evolution of the black hole mass is shown in Fig. 5. We took 800 and 1000 grid points for the lower and higher resolutions, respectively. Since the results for the lower resolution almost overlap the results of the higher resolution, we conclude that the results are convergent. The fitting line for each result is shown as the yellow thick line. The fitting is performed only within a finite time interval shown in Fig. 5. Even though the fitting is performed in the limited region, the formula fits well with the numerical result beyond the fitting region. This result implies that the time evolution of the PBH generated from the isocurvature perturbation can be well described by that in the case of the purely radiation-dominated Universe. The values of the fitting parameters are summarized in Table I. The values of F are clearly larger than those reported in Refs. [15,23]. This discrepancy is perhaps due to the difference in the foliation of the time slices [24]. A simple discussion about the time slice dependence of F is given in the Appendix.

E. Behavior near the threshold

As is shown in the previous sections, the contribution of the massless scalar field is negligible at the time of the horizon formation. Therefore, we expect that the mass of the black hole obeys the critical mass scaling [8,9,11,25–31]

with the critical exponent $\gamma \simeq 0.3558$ [26].[4] It is known that, in order to find the critical exponent in the PBH formation, we need to resolve the horizon formation over more than a few orders of magnitude in the resultant black hole mass. In order to achieve this resolution, we implemented fixed mesh refinement around the center. We introduced at most eight layers depending on the resolution requirement for resolving the black hole formation.

In Fig. 6, we show the mass of the black hole at the moment of the horizon formation as a function of the initial amplitude of the massless scalar field. We performed the fitting by using lower 10 data points shown in Fig. 6 where the scaling relation seems to be realized. The thick orange line in Fig. 6 shows the line with $\gamma = 0.3558$ while the blue solid line is the fitted line without assuming the value of the exponent γ, where the best fit value of γ is given by 0.3562. The threshold value given by the fitting is $\mu_{\text{th}} \simeq 0.63108724$. Our results show good agreement with the critical scaling in the radiation dominated Universe.

IV. SUMMARY AND DISCUSSION

We studied the PBH formation from an isocurvature perturbation of a massless scalar field in the radiation-dominated Universe. Deriving the general growing mode

_____

[4]One should keep in mind that the critical scaling analysis can be done only under the assumption of spherical symmetry. Whether a similar scaling holds in a realistic cosmological situation is an unresolved issue.

solution of the isocurvature perturbation to second order in spatial gradient expansion, we performed numerical simulations of the PBH formation starting from a spherically symmetric Gaussian spatial profile of the scalar field. Even though there is no contribution of the massless scalar field to the stress-energy tensor at leading order, the growing mode solution generally contains the nontrivial metric perturbation at second order, which may consequently lead to nonlinear dynamics of the geometry after the horizon entry. We actually found that a PBH can form for a sufficiently large initial amplitude of the isocurvature perturbation.

We found that although the PBH formation is originally caused by the scalar field isocurvature perturbation, the radiation fluid dominates the dynamics during the gravitational collapse. As a result, the evolution of the PBH mass due to the accretion and the critical behavior near the threshold mass show similar behaviors to those in the standard PBH formation in the radiation-dominated Universe. These facts imply that all the constraints on the curvature perturbation through the observational upper limits of PBH abundance can apply to the case of the isocurvature perturbation of the massless scalar field, and we can obtain similar observational constraints on it.

In this paper, we considered the radiation fluid and a massless scalar field for the matter components as a first step of various possibilities. It would be interesting to consider a scalar field with a nontrivial potential term which introduces additional physical scales, and a rich variety of dynamics across the horizon entry may be expected [32]. The simulation of the PBH formation from the dark matter isocurvature [5], for which nonspherical dynamics may be essential, would be also interesting although such a simulation is much more challenging as one cannot assume spherical symmetry. There are many other fascinating directions to be explored. The current work is just the beginning of these unexplored research themes.

ACKNOWLEDGMENTS

APPENDIX: TIME SLICE DEPENDENCE OF *F*

Let us introduce the effective time t_h near the horizon as follows:

$$t_h = \alpha_h t_c, \tag{A1}$$

here and hereafter, the subscripts "$_h$" and "$_c$" represent the variables for the near horizon region and the cosmological background, respectively. α_h is the lapse function near the horizon and α_c is set to 1. We consider α_h as a constant for simplicity. The density scales as $\rho \propto t^{-2}$, therefore we can define the effective density near the horizon as

$$\rho_h = \alpha_h^{-2} \rho_c. \tag{A2}$$

Then, considering the differential equation of the black hole mass around the horizon,

$$\frac{dM}{dt_h} = 4\pi F_h (2M)^2 \rho_h, \tag{A3}$$

we obtain

$$\frac{dM}{dt_c} = 4\pi \frac{F_h}{\alpha} (2M)^2 \rho_c. \tag{A4}$$

Therefore, the effective coefficient F_c is given by

$$F_c = \frac{F_h}{\alpha}. \tag{A5}$$

Since what we see by the fitting is the value of F_c, the simple analysis suggests the inverse correlation between the lapse function near the horizon and the fitting parameter F.

[1] S. Hawking, Gravitationally collapsed objects of very low mass, Mon. Not. R. Astron. Soc. **152**, 75 (1971).

[2] B. J. Carr and S. Hawking, Black holes in the early Universe, Mon. Not. R. Astron. Soc. **168**, 399 (1974).

[3] B. Carr, K. Kohri, Y. Sendouda, and J. Yokoyama, Constraints on primordial black holes, Rep. Prog. Phys. **84**, 116902 (2021).

[4] B. Carr and F. Kuhnel, Primordial black holes as dark matter: Recent developments, Annu. Rev. Nucl. Part. Sci. **70**, 355 (2020).

[5] S. Passaglia and M. Sasaki, Primordial black holes from CDM isocurvature perturbations, Phys. Rev. D **105**, 103530 (2022)..

[6] G. Domènech, S. Passaglia, and S. Renaux-Petel, Gravitational waves from dark matter isocurvature, J. Cosmol. Astropart. Phys. 03 (2022) 023.

[7] M. Shibata and M. Sasaki, Black hole formation in the Friedmann universe: Formulation and computation in numerical relativity, Phys. Rev. D **60,** 084002 (1999).

[8] J. C. Niemeyer and K. Jedamzik, Dynamics of primordial black hole formation, Phys. Rev. D **59,** 124013 (1999).

[9] I. Musco, J. C. Miller, and L. Rezzolla, Computations of primordial black hole formation, Classical Quantum Gravity **22,** 1405 (2005).

[10] A. G. Polnarev and I. Musco, Curvature profiles as initial conditions for primordial black hole formation, Classical Quantum Gravity **24,** 1405 (2007).

[11] I. Musco, J. C. Miller, and A. G. Polnarev, Primordial black hole formation in the radiative era: Investigation of the critical nature of the collapse, Classical Quantum Gravity **26,** 235001 (2009).

[12] A. G. Polnarev, T. Nakama, and J. Yokoyama, Self-consistent initial conditions for primordial black hole formation, J. Cosmol. Astropart. Phys. 09 (2012) 027.

[13] T. Nakama, T. Harada, A. G. Polnarev, and J. Yokoyama, Identifying the most crucial parameters of the initial curvature profile for primordial black hole formation, J. Cosmol. Astropart. Phys. 01 (2014) 037.

[14] I. Musco, Threshold for primordial black holes: Dependence on the shape of the cosmological perturbations, Phys. Rev. D **100,** 123524 (2019).

[15] A. Escrivà, Simulation of primordial black hole formation using pseudo-spectral methods, Phys. Dark Universe **27,** 100466 (2020).

[16] A. Escrivà, C. Germani, and R. K. Sheth, Universal threshold for primordial black hole formation, Phys. Rev. D **101,** 044022 (2020).

[17] C.-M. Yoo, T. Harada, and H. Okawa, Threshold of primordial black hole formation in nonspherical collapse, Phys. Rev. D **102,** 043526 (2020).

[18] T. Harada, C.-M. Yoo, T. Nakama, and Y. Koga, Cosmological long-wavelength solutions and primordial black hole formation, Phys. Rev. D **91,** 084057 (2015).

[19] C.-M. Yoo, T. Ikeda, and H. Okawa, Gravitational collapse of a massless scalar field in a periodic box, Classical Quantum Gravity **36,** 075004 (2019).

[20] M. Alcubierre, B. Brügmann, D. Holz, R. Takahashi, S. Brandt, E. Seidel, and J. Thornburg, Symmetry without symmetry: Numerical simulation of axisymmetric systems using Cartesian grids, Int. J. Mod. Phys. D **10,** 273 (2001).

[21] Y. B. Zel'dovich and I. D. Novikov, The hypothesis of cores retarded during expansion and the hot cosmological model, Sov. Astron. **10,** 602 (1967).

[22] P. S. Custodio and J. E. Horvath, Evolution of a primordial black hole population, Phys. Rev. D **58,** 023504 (1998).

[23] H. Deng, J. Garriga, and A. Vilenkin, Primordial black hole and wormhole formation by domain walls, J. Cosmol. Astropart. Phys. 04 (2017) 050.

[24] A. Escrivà (private communication).

[25] M. W. Choptuik, Universality and Scaling in Gravitational Collapse of a Massless Scalar Field, Phys. Rev. Lett. **70,** 9 (1993).

[26] T. Koike, T. Hara, and S. Adachi, Critical Behavior in Gravitational Collapse of Radiation Fluid: A Renormalization Group (Linear Perturbation) Analysis, Phys. Rev. Lett. **74,** 5170 (1995).

[27] J. C. Niemeyer and K. Jedamzik, Near-Critical Gravitational Collapse and the Initial Mass Function of Primordial Black Holes, Phys. Rev. Lett. **80,** 5481 (1998).

[28] J. Yokoyama, Cosmological constraints on primordial black holes produced in the near critical gravitational collapse, Phys. Rev. D **58,** 107502 (1998).

[29] A. M. Green and A. R. Liddle, Critical collapse and the primordial black hole initial mass function, Phys. Rev. D **60,** 063509 (1999).

[30] F. Kuhnel, C. Rampf, and M. Sandstad, Effects of critical collapse on primordial black-hole mass spectra, Eur. Phys. J. C **76,** 93 (2016).

[31] I. Musco and J. C. Miller, Primordial black hole formation in the early universe: Critical behaviour and self-similarity, Classical Quantum Gravity **30,** 145009 (2013).

[32] E. de Jong, J. C. Aurrekoetxea, and E. A. Lim, Primordial black hole formation with full numerical relativity, J. Cosmol. Astropart. Phys. 03 (2022) 029.